Strain-Induced Modulation of Electron Mobility in Single-Layer Transition Metal Dichalcogenides MX2 (M = Mo, W; X = S, Se)

Strain Induced Mobility Modulation of Single-Layer Transition Metal Dichalcogenides MX_2 (M = Mo, W; X = S, Se)

Manouchehr Hosseini, Mohammad Elahi, Mahdi Pourfath *Senior Member, IEEE*, and David Esseni *Fellow Member, IEEE*

Abstract

In this paper, the effect of biaxial strain on the mobility of single-layer transition metal dichalcogenides (MoS_2, $MoSe_2$, WS_2, WSe_2) is investigated by accounting for the scattering from intrinsic phonon modes, remote phonons, and charged impurities. Ab-initio simulations are employed to study strain induced effect on the electronic bandstructure and the linearized Boltzmann transport equation is used to evaluate the low-field mobility. The results indicate that tensile strain increases the mobility. In particular, a significant increase in the mobility of single layer $MoSe_2$ and WSe_2 with a relatively small tensile strain is observed. Under compressive strain, however, the mobility exhibits a non-monotonic behavior. With a relatively small compressive strain the mobility decreases and then it partially recovers with further increase in compressive strain.

Index Terms

strain, mobility, Boltzmann transport equation, transition metal dicalcogenides.

I. Introduction

Graphene is the most prominent of two-dimensional material that is attractive for use in next-generation nanoelectronic devices because of its high mobility [1, 2], however, the absence of an energy gap seriously jeopardizes the usage of this material for some important electronic applications, including digital circuits [3, 4]. Other two-dimensional materials with non-zero bandgap, such as single and few-layers of transition metal dichalcogenides (TMDs) offer promising electrical and optical

Manuscript received May 4th, 2015. The review of this manuscript was arranged by Editor ....

M. Hosseini and M. Elahi are with the School of Electrical and Computer Engineering, University of Tehran, Tehran 14395-515 Iran

M. Pourfath is with the School of Electrical and Computer Engineering, University of Tehran, Tehran 14395-515, Iran (pourfath@ut.ac.ir). He is also with the Institute for Microelectronics, Technische Universität Wien, Gußhausstraße 27–29/E360, A-1040 Wien, Austria (pourfath@iue.tuwien.ac.at).

D. Esseni is with DIEGM, Via delle Scienze 206, 33100 Udine, Italy (david.esseni@uniud.it)

properties for future electronic applications [5]. Because of the weak interlayer van der Waals bonds in the layered structure, single to few-layers of these materials can be easily obtained by mechanical or chemical exfoliation techniques [6–8]. n-type field-effect transistors (FETs) based on TMDs have demonstrated a high $I_{\rm on}/I_{\rm off}$ ratio, a relatively steep sub-threshold swing, and an extremely small off-current [9–13]. Possible application of these materials to hetero-junction interlayer tunneling FETs have also been proposed and theoretically investigated [14].

The effect of strain on the bandstructure and bandgap of some of these materials has been investigated in previous studies [15, 16] and it has been shown that the application of compressive and tensile biaxial strain results in an indirect bandgap [17–19]. We have recently studied the effect of strain on the mobility of single layer MoS_2 and shown that tensile biaxial strain can significantly enhance the mobility [20], however, investigation of strain effect on the mobility of other TMDs is still missing. The electronic bandstructures of TMDs are similar, but the valleys have different effective masses and energy minima. In this work, we present a comprehensive analysis on the effect of strain on the electronic bandstructure of TMDs, employing ab-initio simulations and the linearized Boltzmann transport equation (BTE) is solved for evaluating the mobility of these materials [21]. The parameters for ab-initio calculations, scattering rates, and the discretization method of the linearized BTE are briefly presented in Sec. II. The effects of biaxial strain on the bandstructure and mobility of MoS_2, $MoSe_2$, WS_2, and WSe_2 are discussed in Sec. III and concluding remarks are presented in Sec. IV.

II. Modeling Approach

The section explains the approach for the evaluation of the electronic bandstructure and mobility.

A. Bandstructure

For bandstructure calculations we employed the density-functional theory (DFT) along with the local density approximation (LDA) as implemented in the SIESTA code [22]. A 30 Å vacuum region has been used to isolate the single layer from other layers to ensure no interactions between them, thus making our calculations effectively representative of an isolated two-dimensional layer. A cutoff energy equal to 400 Ry was used and the sampling of the reciprocal space Brillouin zone (BZ) is performed by a Monkhorst-pack grid of $18 \times 18 \times 1$ k-points. Calculations begin with the determination of the optimized geometry, that is the configuration in which the residual Hellmann-Feynman forces acting on atoms are smaller than 0.01 eV/Å. The calculated lattice constants of unstrained single-layer MoS_2, $MoSe_2$, WS_2, WSe_2 are 3.12, 3.24, 3.14, 3.26 Å, respectively, which are in agreement with previously reported values in Ref. [23].

Fig. 1(a)-(d) show the bandgaps of these materials in the absence of strain are direct and their values are evaluated to be 1.89, 1.66, 1.98, 1.72 eV, respectively, which are close to the values reported in Ref. [23]. The lowest and second lowest band

minima in the conduction band are denoted as K and Q-valley (see Fig. 2(a)), respectively, and the energy distance between these valleys are evaluated to be 195 meV, 72 meV, 166 meV, 48 meV, for unstrained single-layer MoS_2, $MoSe_2$, WS_2, WSe_2, respectively. A wide range of values for the energy distance between the K and Q-valley has been reported in several theoretical studies [23–25] and no experimental verification has been yet reported except for MoS_2 [26].

B. Scattering Mechanisms and Mobility Calculation

In our calculations carrier scattering due to intrinsic phonons (including acoustic, optical, and polar-optical phonons), remote phonons, and charged impurities are taken into account and piezoelectric coupling to the acoustic phonons is neglected in this work as it is only important at low temperatures [29]. By assuming $\Psi_{\vec{k}}(\vec{r},z) = \chi(z)\exp\left(i\vec{k}.\vec{r}\right)/\sqrt{S}$ with $\chi(z) = \sqrt{(2/a)}\sin(\pi z/a)$ for the envelope function of mobile electrons [30], where $\vec{r}$ is the in-plane position vector, and using Fermi's golden rule the scattering rate from an initial state $\vec{k}$ in valley v to the final state $\vec{k'}$ in valley w can be written as

$$S^{v,w}(\vec{k},\vec{k'}) = \frac{2\pi}{\hbar}|M^{v,w}(\vec{k},\vec{k'})|^2\delta[E^w(\vec{k'}) - E^v(\vec{k}) \mp \hbar\omega(q)] \ , \tag{1}$$

where $|M^{v,w}(\vec{k},\vec{k'})|$ is the matrix element for the mentioned transition and $\hbar\omega(q)$ is the phonon energy that may depend on $q = |\vec{k} - \vec{k'}|$. The intra-valley transitions ($v = w$) assisted by acoustic phonons can be approximated as elastic and the rate is given by

$$S_{\rm ac}(\vec{k},\vec{k'}) = \frac{2\pi k_{\rm B}TD_{\rm ac}^2}{\rho S\hbar v_s^2}\delta[E(\vec{k'}) - E(\vec{k})] \ , \tag{2}$$

where $k_{\rm B}$ is the Boltzmann constant, T is the absolute temperature, $D_{\rm ac}$ is the acoustic the deformation potential, ρ is the mass density and v_s is the sound velocity of single layer TMDs [27, 28]. On the other hand, the rate of inelastic phonon scattering, including intra and inter-valley optical phonons, and inter-valley acoustic phonons, can be expressed as

$$\begin{aligned} S_{\rm ac/op}^{v,w}(\vec{k},\vec{k'}) &= \frac{\pi(D_{\rm ac/op}^{v,w})^2}{\omega_{\rm ac/op}\rho S} \\ &\times \left[n_{\rm op} + \frac{1}{2} \mp \frac{1}{2}\right]\delta[E^w(\vec{k'}) - E^v(\vec{k}) \mp \hbar\omega_{\rm ac/op}(q)] \ , \end{aligned} \tag{3}$$

where $D_{\rm ac/op}^{v,w}$ is the acoustic/optical deformation potential for a transition between valley v and w, $\hbar\omega_{\rm ac/op}(q)$ is the phonon energy, and $n_{\rm op}$ is the phonon occupation (upper and lower sign denote phonon absorption and phonon emission, respectively). There are 6 Q-valleys in the first Brillouin zone and phonon assisted inter-valley transitions correspond to quite different phonon wave vector $q = |\vec{k} - \vec{k'}|$. The corresponding phonon wave vectors are shown in Fig. 2(b) and (c) and for intrinsic phonon scatterings, we adopted the deformation potentials and phonon energies from Ref. [27, 28], that for completeness are reported in Table I and Table II.

Remote phonon or surface-optical (SO) phonon is another important scattering source that can severely degrade electron mobility. The source of this scattering is in the surrounding dielectrics via long-range Coulomb interactions, provided that

the dielectrics support polar vibrational modes. By assuming semi-infinite oxides and neglecting the possible coupling to the plasmons of the two-dimensional material, the energy dispersion of SO phonons can be obtained by solving the secular equation [31]

$$\begin{aligned}(\epsilon_{\rm box}(\omega)+\epsilon_{\rm 2D})(\epsilon_{\rm tox}(\omega)+\epsilon_{\rm 2D})\\ -(\epsilon_{\rm box}(\omega)-\epsilon_{\rm 2D})(\epsilon_{\rm tox}(\omega)-\epsilon_{\rm 2D})e^{-2qa}=0\ ,\end{aligned} \tag{4}$$

where a and $\epsilon_{\rm 2D}$ are respectively the thickness [32–34] and the dielectric constant [35] of the two-dimensional material (single layer TMDs in this work), the index box and tox denote the back-oxide and the top-oxide, respectively. A numerical solution of Eq. (4) shows that the frequency of remote phonon has a very weak dependence on q, that consequently we neglected in our calculations by setting $e^{-2qa}\approx 1$ in Eq. (4). With this approximation, Eq. (4) simplifies to $\epsilon_{\rm box}(\omega)+\epsilon_{\rm tox}(\omega)=0$, that we solved by using the single polar phonon expression for the $\epsilon_{\rm ox}(\omega)$ in each oxide:

$$\epsilon_{\rm ox}(\omega)=\epsilon^{\infty}+\frac{\epsilon^{0}-\epsilon^{\infty}}{1-\omega^2/\omega^2_{\rm TO}}\ , \tag{5}$$

where ϵ^{∞} and ϵ^{0} are the high and low frequency dielectric constant, respectively, and $\omega_{\rm TO}$ is the frequency of the polar phonon in the oxide. We could provide analytical solution for Eq. (5) and express $\omega_{\rm SO,box}$ as: $\omega^2_{\rm SO,box}=(-B+\sqrt{B^2-4AC})/(2A)$ and for $\omega_{\rm SO,tox}$ as $\omega^2_{\rm SO,tox}=(-B-\sqrt{B^2-4AC})/(2A)$, where $A=(\epsilon^{\infty}_{\rm tox}+\epsilon^{\infty}_{\rm box})$, $B=-(\epsilon^{0}_{\rm tox}+\epsilon^{\infty}_{\rm box})\omega^2_{\rm TO,tox}-(\epsilon^{0}_{\rm box}+\epsilon^{\infty}_{\rm tox})\omega^2_{\rm TO,box}$ and $C=(\epsilon^{0}_{\rm tox}+\epsilon^{0}_{\rm box})\omega^2_{\rm TO,tox}\omega^2_{\rm TO,box}$. The parameters of dielectric materials that are studied in this work and the corresponding calculated SO phonon frequencies are reported Table III.

The scattering matrix element of remote phonon can be written as:

$$\begin{aligned}M_{\rm SO,tox}(\vec{k},\vec{k'})=\sqrt{\frac{\hbar\omega_{\rm SO,tox}}{2Sq}}\\ \times\sqrt{\left(\frac{1}{\epsilon^{\infty}_{\rm tox}+\epsilon_{\rm box}(\omega_{\rm SO,tox})}-\frac{1}{\epsilon^{0}_{\rm tox}+\epsilon_{\rm box}(\omega_{\rm SO,tox})}\right)}\ ,\end{aligned} \tag{6}$$

where $\omega_{\rm SO,tox}$ and $\omega_{\rm SO,box}$ are frequency of SO phonon from top and back-oxide, ϵ^{∞} and ϵ^{0} are the high and low frequency dielectric constant and S is the normalization area [31]. The scattering matrix element of remote phonon from back-oxide is obtained by exchanging the subindex of tox and box in Eq. (6). Scattering with SO phonon mode is inelastic and we consider only intra-valley transitions.

Charged impurities located in the center of the two-dimensional material are another source for intra-valley scattering. The Fourier transform of the scattering potential due to a charged impurity located at $(\vec{r},z)=(0,a/2)$ can be written as [38]

$$\phi(q,z)=\frac{\rm e^2}{2q\epsilon_{\rm 2D}}\left[e^{-q|z-a/2|}+Ce^{qz}+De^{-qz}\right]\ , \tag{7}$$

where e is the elementary charge, C and D are the parameters that are dependent on the physical properties of dielectrics and

2D material [20, 38]. Thus the matrix elements due to charge impurity scattering take the form:[20]

$$\begin{aligned} M_{\mathrm{cb}}^{(0)}(\vec{k},\vec{k}') =& \frac{e^2}{qa\epsilon_{2\mathrm{D}}}\left(\frac{1}{q}-\frac{q}{q^2+(2\pi/a)^2}\right) \\ & \times\left[\frac{C}{2}\left(e^{qa}-1\right)+\frac{D}{2}\left(1-e^{-qa}\right)-e^{-qa/2}\right] \\ & +\frac{e^2}{qa\epsilon_{2\mathrm{D}}}\left(\frac{1}{q}+\frac{q}{q^2+(2\pi/a)^2}\right) , \end{aligned} \tag{8}$$

In this work, the effect of static screening produced by the electrons in the conduction band is described by using the dielectric function approach [38], so that the screened matrix element $M_{\mathrm{scr}}^{w}(\vec{k},\vec{k}')$ in valley w is obtained by solving the linear problem:

$$M^{v}(q)=\sum_{w}\epsilon^{v,w}(q)M_{\mathrm{scr}}^{w}(q) , \tag{9}$$

where v and $w \in$ K, Q, $M^{v}(q)$ is the unscreened matrix element, and $\epsilon^{v,w}$ is the dielectric matrix which is introduced as:

$$\epsilon^{v,w}(q)=\delta_{v,w}-\frac{e^2}{q(\epsilon_{2\mathrm{D}}+\epsilon_{\mathrm{box}})}\Pi^{w}(q)F^{v,w}(q) , \tag{10}$$

where $\delta_{v,w}$ is the Kronecker symbol (1 if $v=w$, otherwise zero), $\Pi^{w}(q)$ and $F^{v,w}(q)$ are the polarization factor and unit-less screening form factor, respectively [20, 38]. Static screening has been used for the scattering due to charged impurities and SO phonons, while inter-valley phonon transitions are assumed unscreened [20]. Arguments concerning screening for intra-valley acoustic phonons are more subtle and controversial and a thorough discussion for inversion layer systems can be found in Ref. [39]. The screening for intra-valley acoustic phonons has been neglected as has been done in most of the studies concerning the transport in the inversion layer.

As will be discussed in the next section, the bandstructure close to Q-valley is not isotropic and the corresponding mobility shows direction-dependence while the bandstructure close to K-valley is taken isotropic instead. Assuming a non-parabolic dispersion relation $E(1+\alpha E)=\hbar^2k_l^2/2m_l^*+\hbar^2k_t^2/2m_t^*$, the longitudinal m_l^* and transverse m_t^* effective masses and also the non-parabolicity factor α are extracted from the DFT-calculated electronic bandstructure.

The longitudinal direction of Q-valley is neither the armchair nor the zigzag direction. Therefore, θ is introduced as the angle describing the valley orientation with respect to the armchair direction in real space, see Fig. 2(a). Mobility of each valley along the armchair and zigzag direction is given by [38]

$$\mu_A^{(v)}=\mu_{ll}^{(v)}\cos^2\left(\theta_v\right)+\mu_{tt}^{(v)}\sin^2\left(\theta_v\right) , \tag{11}$$

$$\mu_Z^{(v)}=\mu_{ll}^{(v)}\sin^2\left(\theta_v\right)+\mu_{tt}^{(v)}\cos^2\left(\theta_v\right) , \tag{12}$$

where $\mu_A^{(v)}$ and $\mu_Z^{(v)}$ are the mobility of valley v along the armchair and zigzag direction, θ_v is the angle of longitudinal direction of valley v with respect to the armchair direction in real space. Subindices ll and tt denote the longitudinal and transverse direction, respectively. θ_{Q} only weekly depends on biaxial strain and is approximately zero for two of the Q-valleys,

is $\pi/3$ for other two of them, and is $2\pi/3$ for the remaining Q-valleys. Because of isotropic bandstructure close to K-valley, the value of θ_{K} can be arbitrary. With these angles, the mobility of K and Q-valleys can be rewritten as:

$$\mu_A^{(\mathrm{K0})} = \mu_Z^{(\mathrm{K0})} = 2\mu_{ll}^{(\mathrm{K})} = 2\mu_{tt}^{(\mathrm{K})} \ , \tag{13}$$

$$\mu_A^{(\mathrm{Q0})} = \mu_Z^{(\mathrm{Q0})} = 3\mu_{ll}^{(\mathrm{Q})} + 3\mu_{tt}^{(\mathrm{Q})} \ , \tag{14}$$

where $\mu^{(\mathrm{K0})}$ is the mobility due to two K-valleys and $\mu^{(\mathrm{Q0})}$ is the mobility due to six Q-valleys. The factor 2 in Eq. (13) is because of K-valley degeneracy and factor 3 in Eq. (14) is due to the addition of $\cos^2(\theta_v)$ and $\sin^2(\theta_v)$ of 6 Q-valleys that are introduced in Eq. (11) and Eq. (12). The overall mobility do not depend on the direction and is obtained as the average of the mobilities in different valleys weighted by the corresponding electron density [20]. The mobilities have been calculated by solving numerically the linearized BTE according to the approach described in Ref. [20, 21].

Table IV compares our calculated mobilities at various carrier concentrations with the experimental data reported in Ref. [10] for unstrained single-layer MoS_2 embedded between SiO_2 and HfO_2 with impurity density 4×10^{12} at $T = 100$ K, at which the effect of piezoelectric can be ignored [29]. Very good agreement with experimental data validates the bandstructure and mobility models employed in this work.

III. Results and Discussions

Fig. 3(a)-(d) illustrate the bandstructure of unstrained and strained single layer MoS_2, $MoSe_2$, WS_2 and WSe_2. Tensile biaxial strain increases the energy distance between K and Q-valley, whereas under small compressive strain this energy distance is reduced. With further increase of compressive strain Q-valley will be the lowest one and the K-valley will not significantly contribute to the electronic conduction. The reported energy distances between K and Q-valley by several groups are compared in Table V. Except for MoS_2, where the results indicate an energy distance larger than 60 meV, for the other materials this parameter has not been experimentally extracted. Fig. 4 illustrates the evaluated energy minima of the valleys as a function of strain for the discussed materials. A small tensile strain of 0.4% increases the energy distance by more than 150 meV which can effectively enhance the mobility because of the reduction of inter-valley scattering. Compressive strain, however, decreases this energy distance and with a relatively large compressive strain Q-valley becomes the lowest valley. The longitudinal m_l^* and transverse m_t^* effective masses and the non-parabolicity factors α are shown in Fig. 5(a)-(d). The effective masses of unstrained WS_2 and WSe_2 are smaller than that of unstrained MoS_2 and $MoSe_2$. In all cases, tensile strain decreases the effective mass of K-valley while compressive strain reduces the effective mass of the Q-valley.

The strain-dependency of intrinsic phonon limited mobility is presented in Fig. 6(a). There is a general trend for the modulation of mobility with strain for all discussed materials which can be explained by the variation of inter-valley scattering

between K and Q-valley with strain. As the mobility enhancement with tensile strain is due to the reduction of inter-valley scattering, TMDs with a relatively small energy distance between K and Q-valley will show large mobility enhancement with small tensile strain. For example, the energy distances between the valleys for $MoSe_2$ and WSe_2 are 72 meV and 48 meV, respectively, and a tensile strain of 0.4% results in 64% and 296% mobility enhancement in comparison with those of unstrained materials. The mobility enhancement for MoS_2 and WS_2 under the same condition is 9% and 8% which is due to their relatively large energy distance of 195 meV and 166 meV, respectively. The mobilities of WS_2 and WSe_2 are the highest in comparison with other TMDs because of the relatively small effective mass of the Q-valley under tensile strain.

To analysis the strong variation of mobility with a small compressive strain, Fig. 6(b) depicts the fraction of carrier concentration of the K and Q-valleys as a function of strain. As can be seen, under tensile strain Q-valley becomes empty and does not contribute to the electronic conduction, while under compressive strain the carrier concentration of Q-valley increases and this valley contributes mostly to the conduction. As the effective mass of Q-valley is larger than that of K-valley the phonon limited mobility of this valley is smaller than that of K-valley and one observes a mobility reduction with compressive strain, see Fig. 6(c). The minimum of the overall mobility occurs as the energy minima of K and Q-valley get very close to each other and inter-valley scattering peaks.

Fig. 6(d) depicts the mobility in the presence of intrinsic phonon, remote phonon, and charged impurity scattering. The top and back-oxide are assumed to be HfO_2 and SiO_2, respectively, and both carrier and impurity concentrations are 10^{12} cm^{-2}. As charge impurity and remote phonon scattering result in intra-valley transitions which are weakly affected by strain, the mobility enhancement by strain in the presence of these scattering mechanisms is smaller than that only with intrinsic phonon modes. In this case, the mobility enhancements under 0.4% tensile strain are about 5%, 27%, 4% and 84% for MoS_2, $MoSe_2$, WS_2 and WSe_2, respectively.

The room temperature mobility of unstrained and under tensile strain of 0.4% and 5% of the discussed materials at various carrier concentrations are compared in Fig. 7. A relatively small tensile strain of 0.4% only weakly affects the effective mass of the K-valley (lowest valley), while it has a stronger effect on the energy distance of the valleys. Therefore, even this small strain has the largest (smallest) effect on the mobility of single layer WSe_2 (MoS_2) which has the minimum (maximum) energy distance between the valleys. As at higher carrier concentrations remote phonon and charged impurity scattering are strongly screened and intrinsic phonon scattering plays a more significant role on the mobility, the mobility enhancement by strain is more pronounced at relatively high carrier concentrations. The unstrained single layer WSe_2 has the smallest mobility among all of the discussed unstrained materials, while it has the largest mobility enhancement with tensile strain in the range of 0.4% to 5% and it achieves the highest mobility under a tensile strain of 5%.

IV. Conclusion

A theoretical study on the role of strain on the mobility of single-layer MoS_2, $MoSe_2$, WS_2 and WSe_2 is presented. DFT calculations are used to obtain the effective masses and energy minima of the contributing valleys. The linearized BTE is solved for evaluating the mobility, including the effects of intrinsic phonons, remote phonons, and screened charged impurities. The results indicate that, a tensile strain increases the mobility, whereas a compressive strain reduces the mobility. The unstrained mobility and the mobility enhancement with strain strongly depend on the energy distance between the K and Q-valley. A small tensile strain has a higher impact on the mobility of materials with smaller energy distance between valleys, such as $MoSe_2$ and WSe_2. Various energy distance values result in similar mobility characteristics and the only discrepancy is the strain value at which the mobility starts to increase. Therefore, the main conclusion of this work remains valid regardless of the exact value of the energy distance between K and Q-valley. The results pave the way for improving the performance of TMD-based electronic devices by strain engineering.

Acknowledgement

This work has been partly supported by the Iran National Science Foundation (INSF).

References

[1] K. S. Novoselov, A. K. Geim, S. Morozov, D. Jiang, Y. Zhang, S. Dubonos, I. Grigorieva, and A. Firsov, "Electric field effect in atomically thin carbon films," *Science*, vol. 306, no. 5696, pp. 666–669, 2004.

[2] C. Dean, A. Young, I. Meric, C. Lee, L. Wang, S. Sorgenfrei, K. Watanabe, T. Taniguchi, P. Kim, K. Shepard *et al.*, "Boron nitride substrates for high-quality graphene electronics," *Nature Nanotech.*, vol. 5, no. 10, pp. 722–726, 2010.

[3] Y. Zhang, T.-T. Tang, C. Girit, Z. Hao, M. C. Martin, A. Zettl, M. F. Crommie, Y. R. Shen, and F. Wang, "Direct observation of a widely tunable bandgap in bilayer graphene," *Nature*, vol. 459, no. 7248, pp. 820–823, 2009.

[4] P. Gava, M. Lazzeri, A. M. Saitta, and F. Mauri, "Ab initio study of gap opening and screening effects in gated bilayer graphene," *Phys. Rev. B*, vol. 79, no. 16, p. 165431, 2009.

[5] A. Neto and K. Novoselov, "New directions in science and technology: two-dimensional crystals," *Rep. Prog. Phys.*, vol. 74, no. 8, pp. 82 501–82 509, 2011.

[6] K. Novoselov, D. Jiang, F. Schedin, T. Booth, V. Khotkevich, S. Morozov, and A. Geim, "Two-dimensional atomic crystals," *Proc. Nat. Acad. Sci.*, vol. 102, no. 30, pp. 10 451–10 453, 2005.

[7] A. Ayari, E. Cobas, O. Ogundadegbe, and M. S. Fuhrer, "Realization and electrical characterization of ultrathin crystals of layered transition-metal dichalcogenides," *J. Appl. Phys.*, vol. 101, no. 1, pp. 014 507–014 507, 2007.

[8] H. Ramakrishna Matte, A. Gomathi, A. K. Manna, D. J. Late, R. Datta, S. K. Pati, and C. Rao, "MoS_2 and WS_2 analogues of graphene," *Angew. Chem. Int. Ed.*, vol. 122, no. 24, pp. 4153–4156, 2010.

[9] B. Radisavljevic, A. Radenovic, J. Brivio, V. Giacometti, and A. Kis, "Single-layer MoS_2 transistors," *Nature Nanotech.*, vol. 6, no. 3, pp. 147–150, 2011.

[10] B. Radisavljevic and A. Kis, "Mobility engineering and a metal–insulator transition in monolayer MoS_2," *Nature Mater.*, vol. 12, no. 9, pp. 815–820, 2013.

[11] S. Larentis, B. Fallahazad, and E. Tutuc, "Field-effect transistors and intrinsic mobility in ultra-thin $MoSe_2$ layers," *Appl. Phys. Lett.*, vol. 101, no. 22, p. 223104, 2012.

[12] D. Ovchinnikov, A. Allain, Y.-S. Huang, D. Dumcenco, and A. Kis, "Electrical transport properties of single-layer WS_2," *ACS Nano*, vol. 8, no. 8, pp. 8174–8181, 2014.

[13] W. Liu, J. Kang, D. Sarkar, Y. Khatami, D. Jena, and K. Banerjee, "Role of metal contacts in designing high-performance monolayer n-type WSe_2 field effect transistors," *Nano Lett.*, vol. 13, no. 5, pp. 1983–1990, 2013.

[14] M. O. Li, D. Esseni, G. Snider, D. Jena, and H. G. Xing, "Single particle transport in two-dimensional heterojunction interlayer tunneling field effect transistor," *J. Appl. Phys.*, vol. 115, no. 7, p. 074508, 2014.

[15] H. Shi, H. Pan, Y.-W. Zhang, and B. I. Yakobson, "Quasiparticle band structures and optical properties of strained monolayer MoS_2 and WS_2," *Phys. Rev. B*, vol. 87, no. 15, p. 155304, 2013.

[16] H. J. Conley, B. Wang, J. I. Ziegler, R. F. Haglund Jr, S. T. Pantelides, and K. I. Bolotin, "Bandgap engineering of strained monolayer and bilayer MoS_2," *Nano Lett.*, vol. 13, no. 8, pp. 3626–3630, 2013.

[17] S. M. Tabatabaei, M. Noei, K. Khaliji, M. Pourfath, and M. Fathipour, "A first-principles study on the effect of biaxial strain on the ultimate performance of monolayer MoS_2-based double gate field effect transistor," *J. Appl. Phys.*, vol. 113, no. 16, p. 163708, 2013.

[18] J. Feng, X. Qian, C.-W. Huang, and J. Li, "Strain-engineered artificial atom as a broad-spectrum solar energy funnel," *Nature Photon.*, vol. 6, no. 12, pp. 866–872, 2012.

[19] M. Ghorbani-Asl, S. Borini, A. Kuc, and T. Heine, "Strain-dependent modulation of conductivity in single-layer transition-metal dichalcogenides," *Phys. Rev. B*, vol. 87, no. 23, p. 235434, 2013.

[20] M. Hosseini, M. Elahi, M. Pourfath, and D. Esseni, "Strain induced mobility modulation in single-layer MoS_2," *arXiv:1503.01301*, 2015.

[21] A. Paussa and D. Esseni, "An exact solution of the linearized boltzmann transport equation and its application to mobility calculations in graphene bilayers," *J. Appl. Phys.*, vol. 113, no. 9, p. 093702, 2013.

[22] J. M. Soler, E. Artacho, J. D. Gale, A. García, J. Junquera, P. Ordejón, and D. Sánchez-Portal, "The siesta method for ab initio order-n materials simulation," *J. Phys.: Condens. Matter*, vol. 14, no. 11, p. 2745, 2002.

[23] A. Kumar and P. Ahluwalia, "Electronic structure of transition metal dichalcogenides monolayers 1H-MX_2 (M= Mo, W; X= S, Se, Te) from ab-initio theory: new direct band gap semiconductors," *Eur. J. Phys. B*, vol. 85, no. 6, pp. 1–7, 2012.

[24] C.-H. Chang, X. Fan, S.-H. Lin, and J.-L. Kuo, "Orbital analysis of electronic structure and phonon dispersion in MoS_2, $MoSe_2$, WS_2, and WSe_2 monolayers under strain," *Phys. Rev. B*, vol. 88, no. 19, p. 195420, 2013.

[25] A. Ramasubramaniam, "Large excitonic effects in monolayers of molybdenum and tungsten dichalcogenides," *Phys. Rev. B*, vol. 86, no. 11, p. 115409, 2012.

[26] T. Eknapakul, P. D. King, M. Asakawa, P. Buaphet, R.-H. He, S.-K. Mo, H. Takagi, K. M. Shen, F. Baumberger, T. Sasagawa *et al.*, "Electronic structure of a quasi-freestanding MoS_2 monolayer," *Nano Lett.*, vol. 14, no. 3, pp. 1312–1316, 2014.

[27] X. Li, J. T. Mullen, Z. Jin, K. M. Borysenko, M. B. Nardelli, and K. W. Kim, "Intrinsic electrical transport properties of monolayer silicene and MoS_2 from first principles," *Phys. Rev. B*, vol. 87, no. 11, p. 115418, 2013.

[28] Z. Jin, X. Li, J. T. Mullen, and K. W. Kim, "Intrinsic transport properties of electrons and holes in monolayer transition-metal dichalcogenides," *Phys. Rev. B*, vol. 90, no. 4, p. 045422, 2014.

[29] K. Kaasbjerg, K. S. Thygesen, and A.-P. Jauho, "Acoustic phonon limited mobility in two-dimensional semiconductors: Deformation potential and piezoelectric scattering in monolayer MoS_2 from first principles," *Phys. Rev. B*, vol. 87, p. 235312, Jun 2013.

[30] N. Ma and D. Jena, "Charge scattering and mobility in atomically thin semiconductors," *Phys. Rev. X*, vol. 4, no. 1, p. 011043, 2014.

[31] Z.-Y. Ong and M. V. Fischetti, "Theory of remote phonon scattering in top-gated single-layer graphene," *Phys. Rev. B*, vol. 88, p. 045405, 2013.

[32] Q. Yue, J. Kang, Z. Shao, X. Zhang, S. Chang, G. Wang, S. Qin, and J. Li, "Mechanical and electronic properties of monolayer MoS_2 under elastic strain," *Phys. Lett. A*, vol. 376, no. 12, pp. 1166–1170, 2012.

[33] H. Fang, S. Chuang, T. C. Chang, K. Takei, T. Takahashi, and A. Javey, "High-performance single layered WSe_2 p-fets with chemically doped contacts," *Nano Lett.*, vol. 12, no. 7, pp. 3788–3792, 2012.

[34] R. Gordon, D. Yang, E. Crozier, D. Jiang, and R. Frindt, "Structures of exfoliated single layers of ws_2, mos_2, and $mose_2$ in aqueous suspension," *Phys. Rev. B*, vol. 65, no. 12, p. 125407, 2002.

[35] A. Kumar and P. Ahluwalia, "Tunable dielectric response of transition metals dichalcogenides mx_2 (m= mo, w; x= s, se, te): Effect of quantum confinement," *Physica B: Condensed Matter*, vol. 407, no. 24, pp. 4627–4634, 2012.

[36] A. Konar, T. Fang, and D. Jena, "Effect of high-κ gate dielectrics on charge transport in graphene-based field effect transistors," *Phys. Rev. B*, vol. 82, no. 11, p. 115452, 2010.

[37] V. Perebeinos and P. Avouris, "Inelastic scattering and current saturation in graphene," *Phys. Rev. B*, vol. 81, no. 19, p. 195442, 2010.

[38] D. Esseni, P. Palestri, and L. Selmi, *Nanoscale MOS Transistors*. Cambridge: Cambridge University Press, 2011.

[39] M. V. Fischetti and S. E. Laux, "Monte carlo study of electron transport in silicon inversion layers," *Phys. Rev. B*, vol. 48, no. 4, p. 2244, 1993.

TABLE I

PHONON ENERGY FOR INTRA-VALLEY AND INTER-VALLEY TRANSITIONS AT THE K, M, AND Q POINTS OF SINGLE LAYER TMDS. PARAMETERS OF MoS_2 ARE TAKEN FROM REF. [27] AND PARAMETERS OF OTHER MATERIALS ARE FROM REF. [28]. AS DISCUSSED IN REF.[27, 28], THE ENERGY VALUES FOR ACOUSTIC (OPTICAL) PHONON MODES ARE THE AVERAGE OF PHONON ENERGIES OF THE TRANSVERSE AND LONGITUDINAL (TRANSVERSE, LONGITUDINAL, AND HOMO-POLAR) MODES. THE UNIT FOR ALL PHONON ENERGIES IS MEV.

Material	Phonon Mode	Phonon Energy [meV]			
		Γ	K	M	Q
MoS_2	Acoustic	0	26.1	24.2	20.7
MoS_2	Optical	49.5	46.8	47.5	48.1
$MoSe_2$	Acoustic	0	1.82	18.0	15.1
$MoSe_2$	Optical	34.3	32.8	33.7	33.7
WS_2	Acoustic	0	20.5	19.6	17.7
WS_2	Optical	46.8	45.0	45.8	45.9
WSe_2	Acoustic	0	16.8	15.8	12.9
WSe_2	Optical	30.7	29.7	30.0	30.1

TABLE II

DEFORMATION POTENTIALS FOR INELASTIC PHONON ASSISTED TRANSITIONS IN SINGLE LAYER MoS_2, $MoSe_2$, WS_2, WSe_2. THE FIRST AND THE SECOND COLUMN INDICATE THE INVOLVED PHONON MOMENTUM AND THE ACCORDINGLY ELECTRONIC TRANSITION, RESPECTIVELY. PARAMETERS OF MoS_2 ARE TAKEN FROM REF. [27] AND PARAMETERS OF OTHER MATERIALS ARE TAKEN FROM REF. [28]. $D_1^{ac/op}$ IS THE FIRST ORDER ACOUSTIC/OPTICAL DEFORMATION POTENTIAL IN THE UNIT OF [EV] AND $D_0^{ac/op}$ IS THE ZERO ORDER ACOUSTIC/OPTICAL DEFORMATION POTENTIAL IN THE UNIT OF 10^8 [EV/CM].

Phonon	Electron		Deformation Potentials			
			MoS_2	$MoSe_2$	WS_2	WSe_2
Γ	K→K	D_1^{ac}	4.5	3.4	3.2	3.2
Γ	K→K	D_0^{op}	5.8	5.2	3.1	2.3
K	K→K′	D_0^{ac}	1.4	1.8	1.2	1.3
K	K→K′	D_0^{op}	2.0	2.1	1.1	0.8
Q	K→Q	D_0^{ac}	0.93	0.91	0.73	0.82
Q	K→Q	D_0^{op}	1.9	1.7	0.9	0.8
M	K→ Q	D_0^{ac}	4.4	4.5	3.4	5.7
M	K→ Q	D_0^{op}	5.6	5.3	2.7	3.2
Γ	Q → Q	D_1^{ac}	2.8	3.1	1.8	1.9
Γ	Q → Q	D_0^{op}	7.1	7.8	3.4	2.7
Q	Q →Q	D_0^{ac}	2.1	2.2	1.7	2.7
Q	Q →Q	D_0^{op}	4.8	4.3	2.3	1.9
M	Q →Q	D_0^{ac}	2.0	2.2	1.5	1.5
M	Q →Q	D_0^{op}	4.0	5.9	1.9	1.6
K	Q → Q	D_0^{ac}	4.8	4.1	3.7	4.2
K	Q → Q	D_0^{op}	6.5	4.7	3.1	2.5
Q	Q →K/K′	D_0^{ac}	1.5	1.5	1.4	1.6
Q	Q →K/K′	D_0^{op}	2.4	3.0	1.3	1.0
M	Q →K/K′	D_0^{ac}	4.4	4.9	4.0	4.1
M	Q →K/K′	D_0^{op}	6.6	8.3	4.6	2.8

TABLE III

PARAMETERS FOR THE DIELECTRIC MATERIALS TAKEN FROM (A) REF. [36] AND (B) REF. [37] AND CORRESPONDING CALCULATED SO PHONON FREQUENCIES $\hbar\omega_{\mathrm{SO,tox}}$ AND $\hbar\omega_{\mathrm{SO,box}}$. BACK OXIDE IS SiO_2.

Mater.	$SiO_2^{(a)}$	$BN^{(b)}$	$AlN^{(a)}$	$Al_2O_3^{(a)}$	$HfO_2^{(a)}$	$ZrO_2^{(a)}$
$\epsilon^0_{\mathrm{tox}}$	3.9	5.09	9.14	12.53	23	24
$\epsilon^\infty_{\mathrm{tox}}$	2.5	4.1	4.8	3.2	5.03	4
$\omega_{\mathrm{TO,tox}}$	55.6	93.07	81.4	48.18	12.4	16.67
$\omega_{\mathrm{SO,tox}}$ (cal.)	69.4	100.5	104.3	83.9	21.3	30.5
$\omega_{\mathrm{SO,box}}$ (cal.)	69.4	60.1	58.0	54.2	61.1	62.9

TABLE IV

COMPARISON OF THE CALCULATED MOBILITY IN THIS WORK WITH THE EXPERIMENTAL DATA OF REF. [10]. $T = 100$ K AND THE IMPURITY DENSITY IS 4×10^{12} CM^{-2}. THE UNITS OF CARRIER CONCENTRATION (n) AND MOBILITY (μ) ARE CM^{-2} AND $\mathrm{CM}^2/(\mathrm{Vs})$, RESPECTIVELY.

n	7.6×10^{12}	9.6×10^{12}	1.15×10^{13}	1.35×10^{13}
μ (Cal.)	93	106	114	122
μ (Exp.)	96±3	111±3	128±3	132±3

TABLE V

THE ENERGY DISTANCE BETWEEN K AND Q-VALLEY BASED ON THEORETICAL STUDIES IN REFS. [23–25]. THE REPORTED DATA FROM REF.[25] INCLUDE SPIN-ORBIT INTERACTION. THE UNITS ARE MEV.

Mater.	K and Q-Valley Energy Distance [meV]			
	This Study	Ref. [23]	Ref.[24]	Ref.[25]
MoS_2	195	300 ± 30	255 ± 10	115 ± 20 , 190 ± 20
$MoSe_2$	72	370 ± 30	180 ± 10	10 ± 20 , 10 ± 20
WS_2	166	80 ± 30	200 ± 10	10 ± 20 , 255 ± 20
WSe_2	48	220 ± 30	135 ± 10	-80 , 80 ± 20

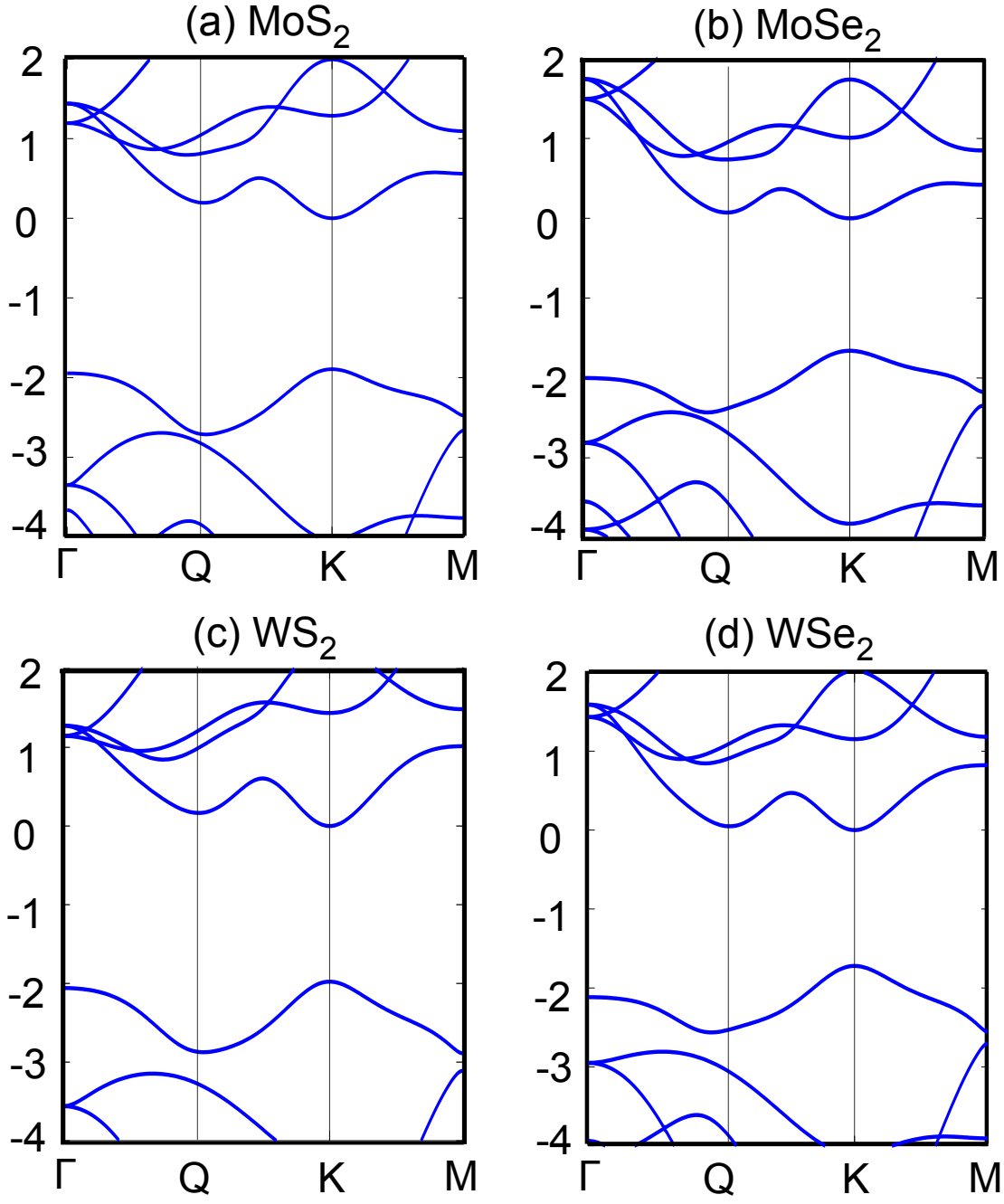

Fig. 1. The electronic bandstructure along high symmetry lines of unstrained single layer: (a) MoS_2; (b) $MoSe_2$; (c) WS_2; (d) WSe_2.

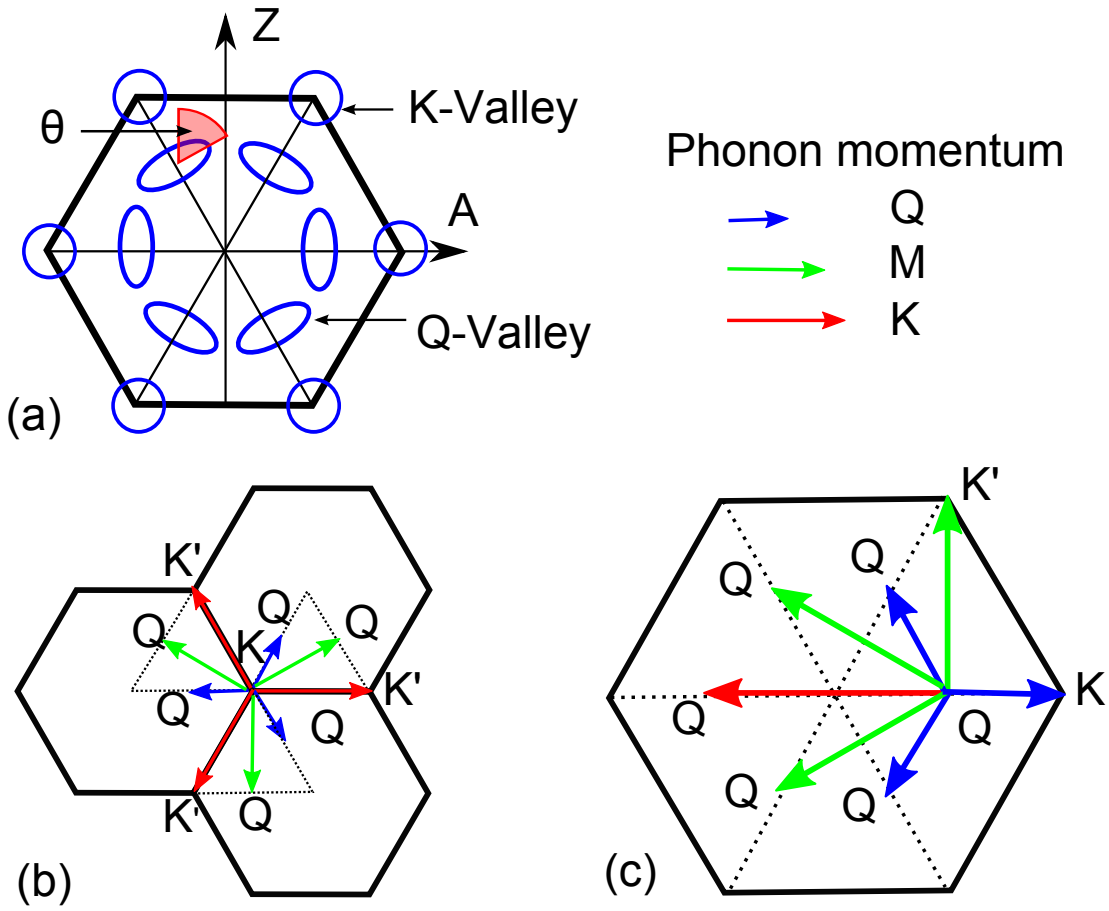

Fig. 2. (a) K and Q-valleys in the first Brillouin zone of TMDs. The angle θ describes the Q-valleys orientation in $\vec{k}$-space. It should be noted that the zigzag direction in $\vec{k}$-space corresponds to the armchair direction in real space. Illustration of several phonon assisted inter-valley transitions in single layer MX_2 for: (b) transitions from K-valley to other valleys; (v) transitions from Q-valley to other valleys. The figure sets the notation used in Table I and Table II to identify phonon assisted transitions.

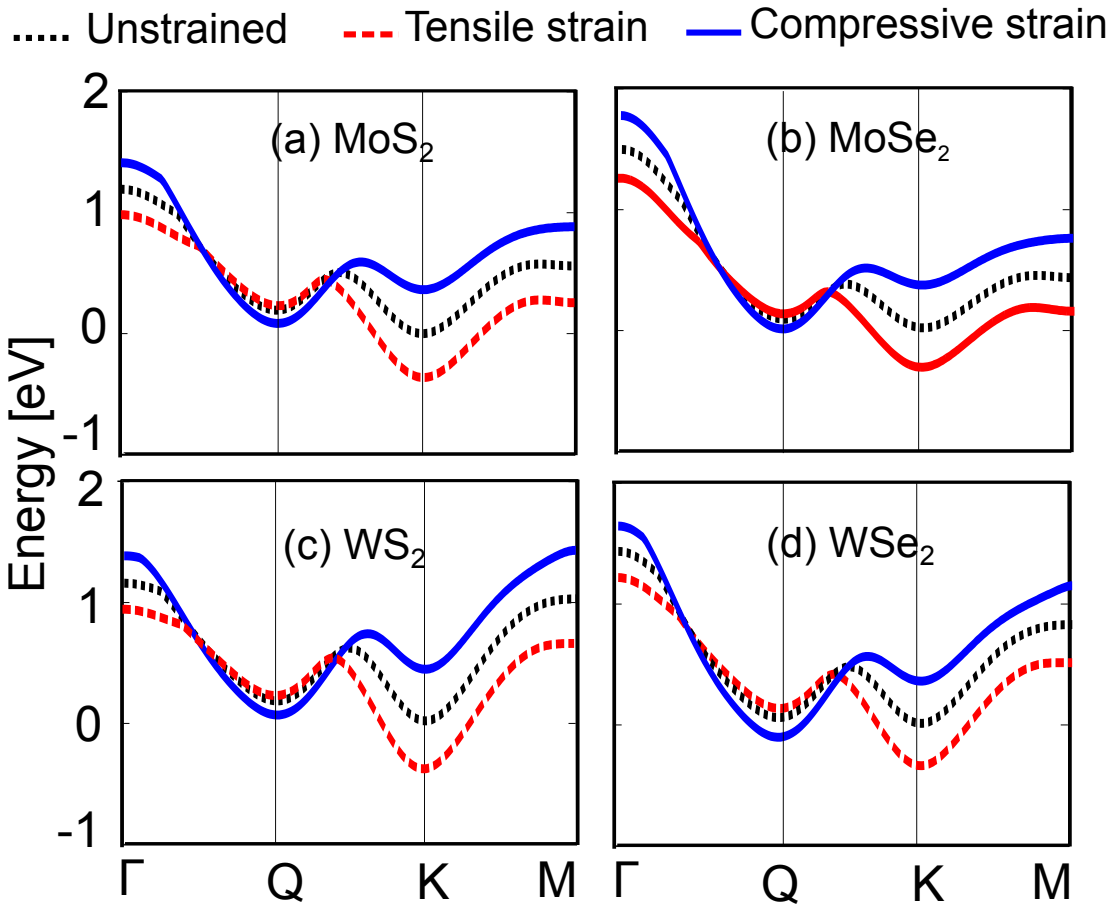

Fig. 3. The band structure of unstrained (black line), under compressive strain (blue line), and under tensile strain (red line) of single layer MoS_2, $MoSe_2$, WS_2, and WSe_2. The strain magnitude is 2.5% in all strained cases.

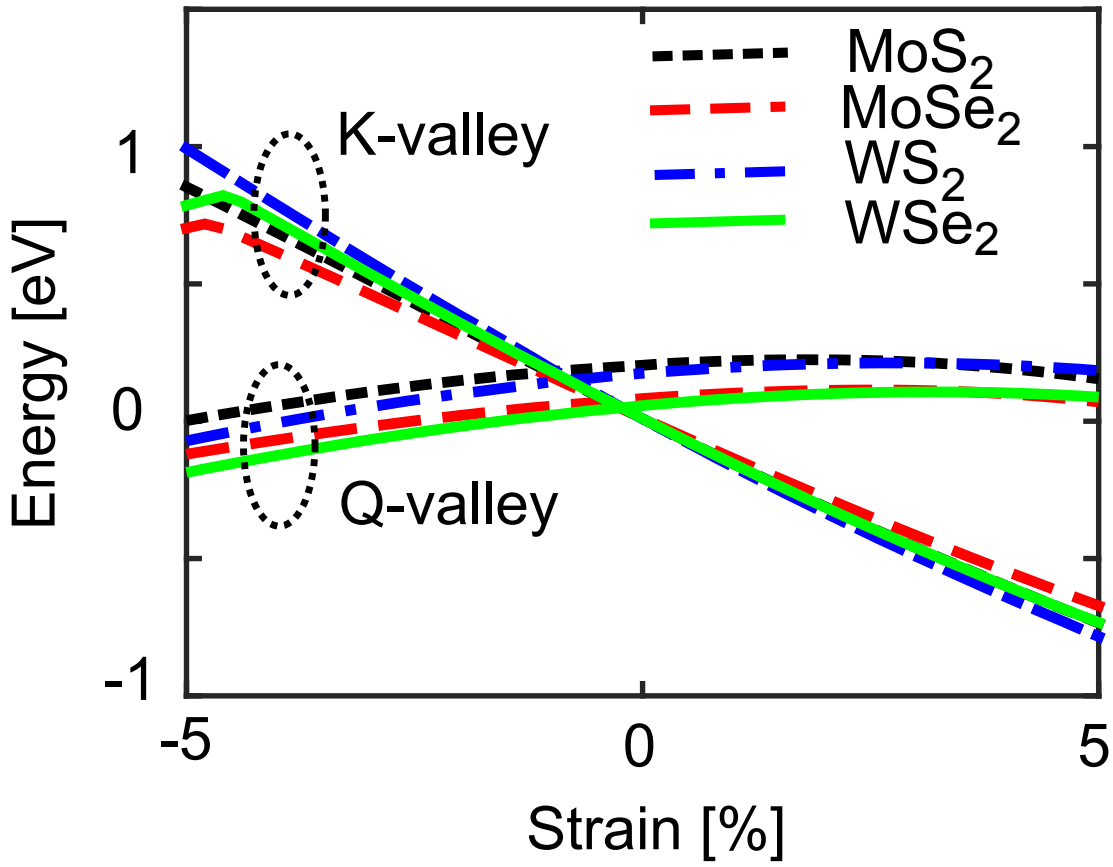

Fig. 4. The energy minima of the K and Q-valley under biaxial strain are illustrated in Fig. 1 for MoS_2 (black), $MoSe_2$ (red), WS_2 (blue), and WSe_2 (green).

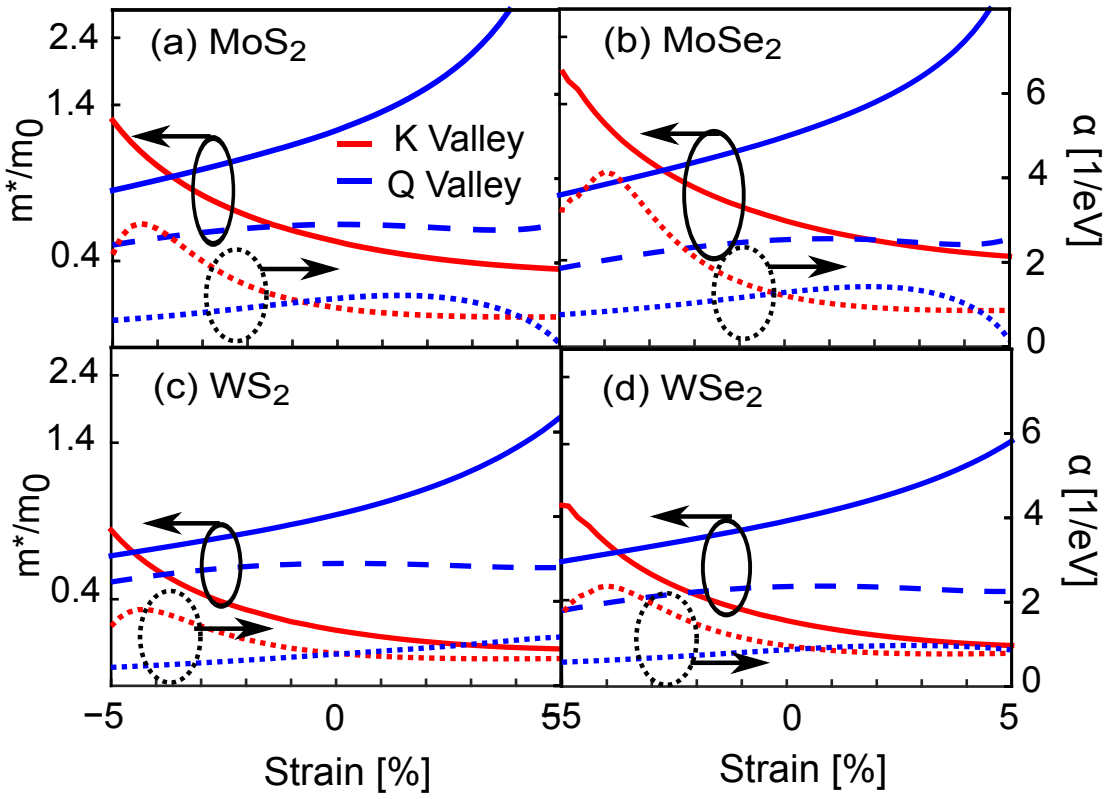

Fig. 5. The effective masses (solid-lines for longitudinal and dashed-lines for transverse directions) and the non-parabolicity factor (α) (dotted-lines) of various valleys (blue line for K-valley and red line for Q-valley) under biaxial strain for: (a) MoS_2; (b) $MoSe_2$; (c) WS_2; (d) WSe_2. The longitudinal and transverse effective masses of K-valley are assumed to be equal.

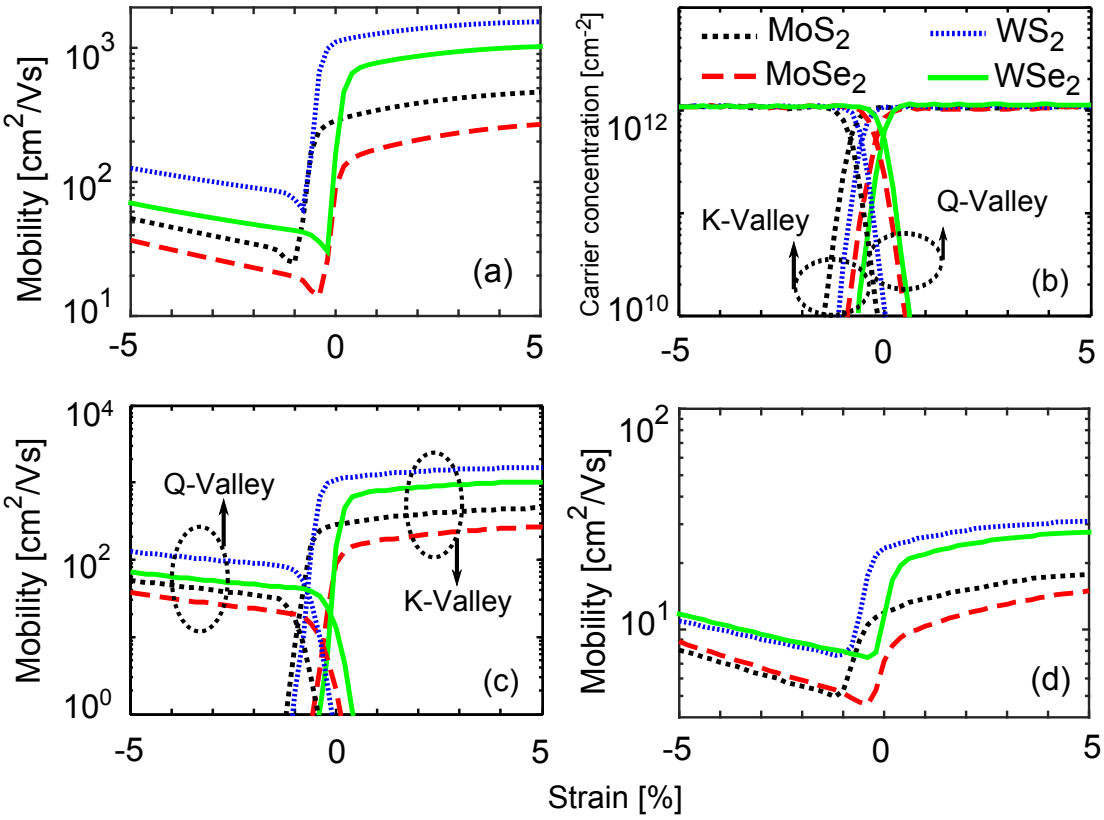

Fig. 6. (a) Phonon limited mobility of single layer TMDs as a function of strain with a carrier concentration of $n = 10^{12}$ cm^{-2}. (b) The fraction of carrier concentration and (c) phonon limited mobility of 2 K-valleys and 6 Q-valleys of single layer TMDs as a function of strain. (d) Mobility limited by intrinsic phonon modes, remote phonon, and screened charged impurity scattering with SiO_2 as the back gate oxide (ϵ_r = 3.9) and HfO_2 as the top gate oxide (ϵ_r = 23). Carrier and charged impurity concentrations are equal to $n = n_{imp} = 10^{12}$ cm^{-2}. Black, red, blue, and green lines illustrate the mobility of MoS_2, $MoSe_2$, WS_2, and WSe_2, respectively.

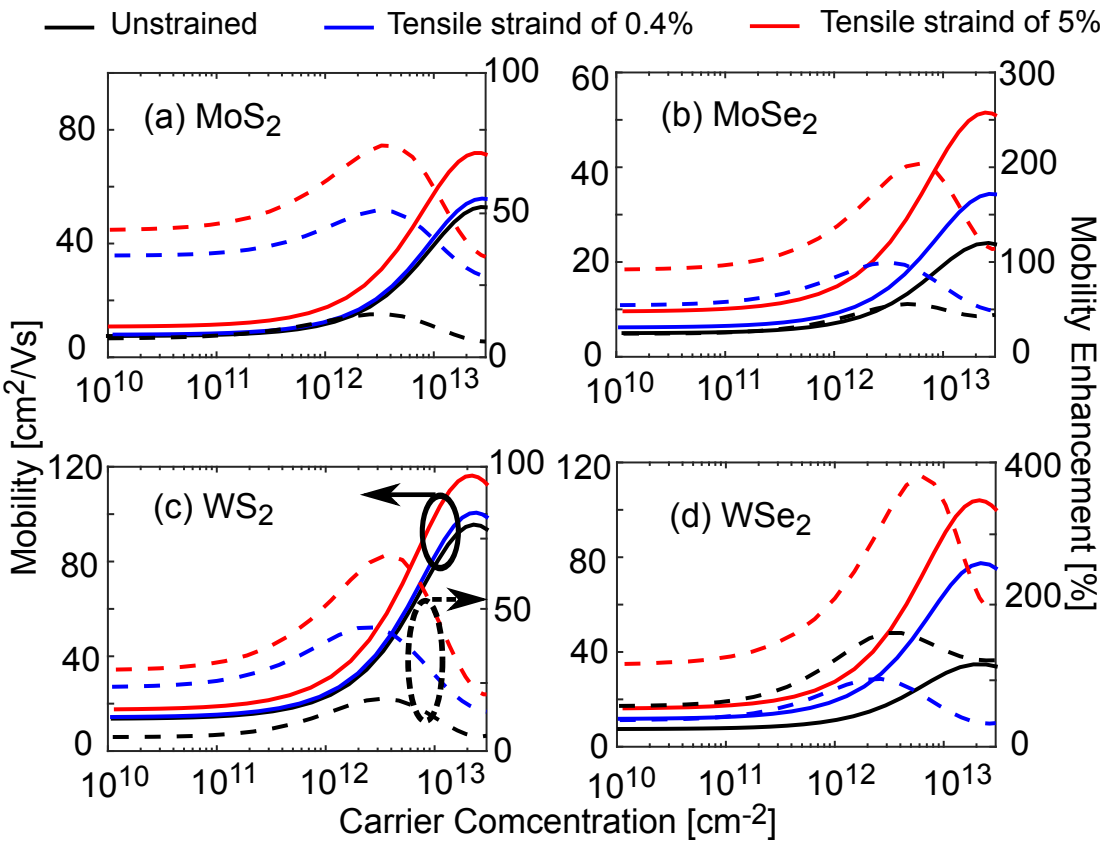

Fig. 7. The mobility (solid lines) and mobility enhancement (dashed lines) with the inclusion of intrinsic phonon, remote phonon, and charged impurity scattering for the unstrained (black), under a tensile biaxial strain of 0.4% (blue), under a tensile biaxial strain of 5% (red) for: (a) MoS_2; (b) $MoSe_2$; (c) WS_2; (d) WSe_2. Top and back-oxide are HfO_2 and SiO_2, respectively, and the charge impurity concentration is equal to $n_{\rm imp} = 10^{12}$ cm^2. Left axes indicate the mobility and right axes shows the mobility enhancement.